ELSEVIER

Cell Calcium 38 (2005) 73–86

cell calcium

www.elsevier.com/locate/ceca

The dynamics of stochastic attrition viewed as an absorption time on a terminating Markov chain

Hilary DeRemigio, Gregory D. Smith *

Department of Applied Science, McGlothlin-Street Hall, Rm 305, The College of William and Mary, Williamsburg, VA 23187, USA

Received 27 April 2005; received in revised form 31 May 2005; accepted 1 June 2005

Abstract

Localized Ca^{2+} elevations known as Ca^{2+} puffs and sparks are cellular signals that arise from the cooperative activity of clusters of inositol 1,4,5-trisphosphate receptors and ryanodine receptors clustered at Ca^{2+} release sites on the surface of the endoplasmic reticulum or sarcoplasmic reticulum. When Markov chain models of these intracellular Ca^{2+}-regulated Ca^{2+} channels are coupled via a mathematical representation of Ca^{2+} microdomain, simulated Ca^{2+} release sites may exhibit the phenomenon of "stochastic Ca^{2+} excitability" where the inositol 1,4,5-trisphosphate receptors (IP_3Rs) or ryanodine receptors (RyRs) open and close in a concerted fashion. Interestingly, under some conditions simulated puffs and sparks can be observed even when the single-channel model used does not include slow Ca^{2+} inactivation or, indeed, any long-lived closed/refractory state [V. Nguyen, R. Mathias, G. Smith, Stochastic automata network descriptor for Markov chain models of instantaneously-coupled intracellular Ca^{2+} channels, Bull. Math. Biol. 67 (2005) 393–432]. In this case, termination of the localized Ca^{2+} elevation occurs when all of the intracellular channels at a release site simultaneously close through a process referred to as *stochastic attrition* [M. Stern, Theory of excitation-contraction coupling in cardiac muscle, Biophys. J. 63 (1992) 497–517]. In this paper, we investigate the statistical properties of stochastic attrition viewed as an absorption time on a terminating Markov chain that represents a Ca^{2+} release site composed of N two-state channels that are activated by Ca^{2+}. Assuming that the local $[Ca^{2+}]$ experienced by a channel depends only on the number of open channels at the Ca^{2+} release site (i.e., instantaneous mean-field coupling [ibid.], we derive the probability distribution function for the time until stochastic attrition occurs and present an analytical formula for the expectation of this random variable. We explore how the contribution of stochastic attrition to the termination of Ca^{2+} puffs and sparks depends on the number of channels at a release site, the source amplitude of the channels (i.e., the strength of the coupling), the background $[Ca^{2+}]$, channel kinetics, and the cooperactivity of Ca^{2+} binding. Because we explicitly model the Ca^{2+} regulation of the intracellular channels, our results differ markedly from (and in fact generalize) preliminary analyses that assume the intracellular Ca^{2+} channels are uncoupled and consequently independent.
© 2005 Elsevier Ltd. All rights reserved.

Keywords: Stochastic attrition; Calcium puff; Calcium spark; Terminating Markov chain; Absorption time; Puff duration; Spark duration

1. Introduction

Localized Ca^{2+} elevations known as Ca^{2+} 'puffs' and 'sparks' are cellular signals of great interest. Ca^{2+} puffs, sparks, and localized Ca^{2+} elevations due to plasma membrane Ca^{2+} channels are not only the building blocks of global Ca^{2+} release events in eukaryotic cells, but also highly specific regulators of cellular function [3–5,10,11].

The relationship between single-channel kinetics and the dynamics of localized Ca^{2+} release is complicated by the short range of action of intracellular Ca^{2+} [1] and the co-localization of intracellular Ca^{2+} channels at Ca^{2+} release sites on the surface of the endoplasmic reticulum (ER) or sarcoplasmic reticulum (SR). For example, in the cortical regions (approximately 6 μm below the plasma membrane) of immature *Xenopus* oocytes, inositol 1,4,5-trisphosphate receptors (IP_3Rs) occur in clusters of 5–50 with inter-cluster spacing on the order of a few microns [40]. IP_3Rs are also clustered on the surface of the outer nuclear membrane of Xenopus oocytes [19]. Similarly, intracellular Ca^{2+} release in

* Corresponding author. Tel.: +1 757 221 1989; fax: +1 757 221 2050.
E-mail address: greg@as.wm.edu (G.D. Smith).
URL: http://www.as.wm.edu/Faculty/Smith.html.

0143-4160/$ – see front matter © 2005 Elsevier Ltd. All rights reserved.
doi:10.1016/j.ceca.2005.06.007

skeletal and cardiac myocytes is mediated by clusters of ryanodine receptors (RyRs) that are assembled into paracrystaline arrays of approximately 100 cooperatively gating channels [6,14,44].

The spatial organization of IP_3Rs and RyRs is the basis of three distinct modes of Ca^{2+} mobilization that have been observed via confocal microfluorimetry in oocytes, cardiomyocytes, and many other cell types: (1) localized Ca^{2+} elevations due to the activation of a single channel that are referred to as Ca^{2+} blips or quarks depending on whether the event is mediated by IP_3Rs or RyRs [25]; (2) Ca^{2+} elevations due to the activation of multiple channels associated with a single Ca^{2+} release site known as Ca^{2+} puffs and sparks [9,11,27,45]; and (3) global responses such as oscillations and waves that involve multiple release sites [10]. These three modes of Ca^{2+} release have been dubbed fundamental, elementary, and global responses, respectively [4].

Several groups have presented simulations [17,21,24,29,30,32,33,38,41,42] demonstrating that Ca^{2+} puffs and sparks may arise from the cooperative activity of clusters of IP_3Rs and RyRs modeled as a continuous-time discrete-state Markov process (for review of simulation methods see [12,34]). These calculations have established that when single-channel models of Ca^{2+}-regulated Ca^{2+} channels are coupled via a time-dependent or time-independent Ca^{2+} microdomain, simulated Ca^{2+} release sites may exhibit the phenomenon of "stochastic Ca^{2+} excitability" where the IP_3Rs or RyRs open and close in a concerted fashion. Allosteric interactions between intracellular Ca^{2+} channels may lead to synchronization [38], but such direct coupling is not required. Rather, Ca^{2+} sparks and puffs can readily be observed when the coupling between single-channel models is mediated entirely via the buffered diffusion of intracellular Ca^{2+} simulated through solution of a system of non-linear reaction-diffusion equations. In the above mentioned studies, the specific single-channel model chosen, the release site geometry, and the description of the cytosolic milieu are all important components of these simulated puffs and sparks that contribute to measured statistics such as amplitude, duration, and inter-event interval. The IP_3R or RyR models used often include transitions representing fast Ca^{2+} activation and slower Ca^{2+} inactivation, two phenomena that have been repeatedly (but not uniformly) observed in single-channel recordings from planar lipid bilayer and nuclear patch experiments [7,13,15,19,22,28].

Although the biophysical theory relating the single-channel kinetics of IP_3Rs and RyRs to the collective phenomena of Ca^{2+} puffs and sparks is not well-developed, Markov chain models of coupled intracellular Ca^{2+} channels give insight into the factors determining the amplitude, duration, and inter-event intervals of Ca^{2+} puffs and sparks. For example, several investigators have observed a requirement of significant inter-channel communication in the genesis of Ca^{2+} puffs and sparks, that is, low-density Ca^{2+} release sites exhibit a low puff-to-blip ratio or may not exhibit stochastic excitability at all [42]. Another observation is that the stochastic Ca^{2+} excitability exhibited by coupled Ca^{2+} channels that include both Ca^{2+} activation and Ca^{2+} inactivation – e.g., the four-state type 1-like IP_3R model presented in [23] – can be eliminated by modifying Ca^{2+}-inactivation rates. Some single-channel models that include Ca^{2+}-inactivition are not particularly sensitive to the density of channels at the simulated Ca^{2+} release site, so long as the requirement for inter-channel communication is satisfied, while other single-channel models are unable to generate robust puffs regardless of channel density [23].

Interestingly, under some conditions simulated puffs and sparks may occur even when the single-channel model used does not include slow Ca^{2+} inactivation or, indeed, any long-lived closed/refractory state. This has been observed, for example, in a model of IP_3-sensitive Ca^{2+} release sites composed of type 2-like IP_3R models that include Ca^{2+}-activation but not Ca^{2+}-inactivation [23]. Because there are a finite number of intracellular Ca^{2+} channels at a release site, there is always a chance that all of them will close simultaneously, a mechanism referred to as *stochastic attrition* in the context of spark termination in cardiac myocytes [36,37]. Even if Ca^{2+} inactivation or allosteric coupling is the mechanism dominating the termination of a localized Ca^{2+} release event, stochastic attrition is always present and consequently will play some role. But when are the consequences of stochastic attrition negligible? And when are the dynamics of stochastic attrition an important aspect of stochastic Ca^{2+} excitability?

In order to quantify the possible contribution of stochastic attrition to the termination of puffs and sparks, investigators have roughly estimated the rate of termination events (k_{attrit}) in a cluster of N uncoupled (i.e., independent) channels toggling between open and closed states with mean open time τ_O and open probability p_O [36,37]. The reciprocal of this rate gives the so-called "stochastic attrition time constant,"

$$\tau_{\text{attrit}} = \frac{1}{k_{\text{attrit}}} = \tau_O \frac{1-(1-p_O)^N}{N(1-p_O)^{N-1}p_O}, \tag{1}$$

corresponding to the mean time between extinction events where all N channels are closed (see Appendix A). This expression indicates that for fixed open probability and mean open time the stochastic attrition time constant for a cluster of uncoupled two-state channels is an exponentially increasing function of N. For example, Fig. 1 shows that for $p_O = 0.15$ and $\tau_O = 1$ ms, the stochastic attrition time constant is $\tau_{\text{attrit}} = 7$ ms when $N = 20$ (*open circle*), but this value dramatically increases to over 10 min when $N = 100$ (*open square*). If a release site is composed of $N = 100$ uncoupled channels with an open probability of $p_O = 0.2$ and mean open time of $\tau_O = 1$ ms, the stochastic attrition time constant is greater than two days (*filled square*). Thus, a back-of-the-envelope calculation (Eq. (1)) forcefully indicates that the contribution of stochastic attrition to the termination of Ca^{2+} puff and spark events will be minimal.

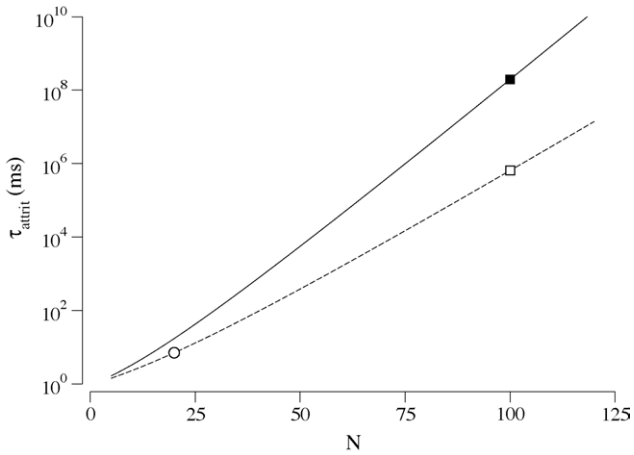

Fig. 1. The time constant for stochastic attrition (τ_{attrit}) as a function of the number (N) of independent two-state channels with mean open time $\tau_O = 1$ ms (Eq. (1)). The *solid* and *dotted* lines correspond to $p_O = 0.20$ and $p_O = 0.15$, respectively. Exponentially increasing values of τ_{attrit} suggest that the contribution of stochastic attrition to the termination of Ca^{2+} sparks and puffs is negligible for release sites composed of uncoupled channels.

This simple statistical demonstration that stochastic attrition is unlikely to contribute to the termination of Ca^{2+} puffs and sparks conflicts with the observation that in some cases stochastic Ca^{2+} excitability is exhibited by simulated Ca^{2+} release sites composed of single-channel models that do not include Ca^{2+} inactivation [24]. The discrepancy is due to the fact that the analytical result (Eq. (1)) assumes that the channels are uncoupled and independent, while the simulations suggesting that stochastic attrition may in some cases be the termination mechanism for Ca^{2+} puffs and sparks are more realistic and more complex. Most importantly, the simulations include Ca^{2+}-regulated Ca^{2+} channels that are coupled with one another through an evolving Ca^{2+} microdomain. Though the channels may be identical, they are not independent because the Ca^{2+} microdomain formed by open channels profoundly influences the subsequent stochastic gating of the release site.

In this paper, we investigate the statistical properties of the phenomenon of stochastic attrition without making the assumption of uncoupled and independent channels. In Sections 2.1 and 2.2, we formulate the problem using a minimal two-state model of a Ca^{2+}-activated Ca^{2+} channel and show how the extinction time of a puff or spark – the time until stochastic attrition occurs – can be viewed as an absorption time on an $N+1$ state Markov chain. This is essentially the same approach as used to derive Eq. (1), except that we explicitly model the Ca^{2+} regulation of the channels and, consequently, the channels do not gate independently. In Section 2.3, we derive the probability distribution function for the time until stochastic attrition and the expectation of this random variable, thus generalizing Eq. (1) to the case of coupled channels. Sections 3.1–3.3 explore how the ability of stochastic attrition to terminate Ca^{2+} puffs and sparks depends on the number of channels at a release site, the source amplitude of the channels (i.e., how strongly they are coupled), the background $[Ca^{2+}]$, and the cooperativity of Ca^{2+} binding.

2. Formulation of model

2.1. A two-state channel model with Ca^{2+} activation

Stochastic models of single-channel gating often take the form of continuous-time discrete-state Markov processes (for review see [12,34]). For example, a transition-state diagram for a two-state channel activated by Ca^{2+} is given by

$$\text{(closed)}\ \ \mathrm{C} \underset{k^-}{\overset{k^+c^\eta}{\rightleftharpoons}} \mathrm{O}\ \ \text{(open)} \tag{2}$$

where k^+c^η and k^- are transition rates with units of reciprocal time, k^+ is an association rate constant with units of conc$^{-\eta}$ time^{-1}, η is the cooperativity of Ca^{2+} binding, and c is the local $[Ca^{2+}]$ that may be either constant or a function of time. If the local $[Ca^{2+}]$ is specified, the transition state diagram of the channel (Eq. (2)) defines a discrete-state continuous-time stochastic process, $S(t)$, that takes on values in the state space $S = (\mathrm{C}, \mathrm{O})$. For example, if the local $[Ca^{2+}]$ is assumed to be a fixed background $[Ca^{2+}]$ denoted by $c = c_\infty$, Eq. (2) corresponds to the well-known telegraph process with an infinitesimal generator or Q-matrix given by [12,26]

$$Q = (q_{ij}) = \begin{pmatrix} -k^+c_\infty^\eta & k^+c_\infty^\eta \\ k^- & -k^- \end{pmatrix} \tag{3}$$

where the off-diagonal elements are transition rates

$$q_{ij} = \lim_{\Delta t \to 0} \frac{P\{S(t+\Delta t) = S_j | S(t) = S_i\}}{\Delta t} \quad (i \neq j) \tag{4}$$

and the diagonal elements are such that each row sum is zero, $\sum_j q_{ij} = 0$. Eq. (3) is important because all of the statistical properties of the two-state channel model diagrammed in Eq. (2) can be derived from this Q-matrix. For example, the probability that the channel is in state j at time $t \geq 0$ given that it was in state i at time $t = 0$ is given by the elements $p_{ij}(t)$ of a matrix $P(t) = e^{tQ}$ that can be calculated from Q using a matrix exponential.

2.2. Instantaneously coupled two-state channels

In order to expand Eqs. (2) and (3) to represent two identical coupled channels, we write c_* as the $[Ca^{2+}]$ above background experienced by the Ca^{2+} regulatory site of channel 2 when channel 1 is open (and vice versa) and assume that channel gating is a process that is slow compared to the time required for the local $[Ca^{2+}]$ to change. This assumption of "instantaneous coupling" [24] allows us to write the transition state diagram for two coupled two-state channels

where both are activated by Ca^{2+} as

$$\begin{array}{ccccc} & & k^+c_\infty^\eta & & \\ & CC & \rightleftharpoons & OC & \\ & & k^- & & \\ k^+c_\infty^\eta \downarrow\uparrow k^- & & & k^- \downarrow\uparrow k^+(c_\infty+c_*)^\eta & \\ & & k^- & & \\ & CO & \rightleftharpoons & OO & \\ & & k^+(c_\infty+c_*)^\eta & & \end{array} \quad (5)$$

Here the expanded state space includes both channels closed (CC), both channels open (OO), or one channel open and the other closed (CO and OC). Note the parameter c_* is added to the background $[Ca^{2+}]$ (c_∞) when either of the two channels makes a C → O transition while the other channel is open, that is, in the CO → OO and OC → OO transitions in Eq. (5). Because the channels are identical, states CO and OC are equivalent and can be combined. This leads to a 3×3 generator matrix corresponding to Eq. (5) where lumping states leads to the doubling of some entries:

$$Q = \begin{pmatrix} -2k^+c_\infty^\eta & 2k^+c_\infty^\eta & 0 \\ k^- & -k^- - k^+(c_\infty+c_*)^\eta & k^+(c_\infty+c_*)^\eta \\ 0 & 2k^- & -2k^- \end{pmatrix} \quad (6)$$

For example, the transition rate out of the CC state is $2k^+c_\infty^\eta$, because either of the closed channels can open leading to the lumped state CO/OC.

Eqs. (5) and (6) indicate how we may derive a minimal model of N stochastically gating two-state channels, each activated by Ca^{2+} as in Eq. (2), providing we assume that the local $[Ca^{2+}]$ experienced by a channel depends only on the number of open channels at the Ca^{2+} release site [24]. When this assumption of mean-field coupling is combined with the prior assumption of instantaneous coupling, we can write the local $[Ca^{2+}]$ experienced by each channel as $c_\infty + N_O c_*$, where c_∞ is the background $[Ca^{2+}]$, c_* is the $[Ca^{2+}]$ above background contributed by any open channel, and N_O is the number of open channels. Thus, a transition-state diagram for a cluster of N coupled two-state channels activated by Ca^{2+} is

$$0 \underset{k^-}{\overset{Nk^+c_0}{\rightleftharpoons}} 1 \underset{2k^-}{\overset{(N-1)k^+c_1}{\rightleftharpoons}} 2 \underset{3k^-}{\overset{(N-2)k^+c_2}{\rightleftharpoons}} \cdots \underset{(N-1)k^-}{\overset{2k^+c_{N-2}}{\rightleftharpoons}} N-1 \underset{Nk^-}{\overset{2k^+c_{N-1}}{\rightleftharpoons}} N \quad (7)$$

where the state of the system $S = (0, 1, \ldots, N)$ indicates the number of open channels, N_O, and the local $[Ca^{2+}]$ used in each Ca^{2+}-mediated transition is a linear function of the number of open channels ($c_n = c_\infty + nc_*$). The Q-matrix corresponding to Eq. (7),

$$Q = \left(\begin{array}{c|cccccc} \diamond & Nk^+c_\infty^\eta & & & & & \\ \hline k^- & \diamond & (N-1)k^+(c_\infty+c_*)^\eta & & & & \\ & 2k_- & \diamond & (N-2)k^+(c_\infty+2c_*)^\eta & & & \\ & & & \ddots & & & \\ & & & & (N-1)k^- & \diamond & k^+(c_\infty+(N-1)c_*)^\eta \\ & & & & & Nk^- & \diamond \end{array}\right), \quad (8)$$

is tridiagonal with the entry q_{ij} giving the rate of transition from a release site with i open channels ($N_O = i$) to a release site where $N_O = j$. The lower diagonal elements of Eq. (8) are unimolecular rate constants while the bimolecular rate constants are included in the $[Ca^{2+}]$-dependent upper diagonal. The diamonds ($\diamond$) in Eq. (8) indicate a diagonal entry leading to a row sum of zero. Notice that the rates of O → C transitions appearing in the lower diagonal are scaled by the number of open channels which increases from $N_O = 1$ to $N_O = N$ in subsequent rows. Conversely, the number of closed channels ($N_C = N - N_O$) that scales the upper diagonal entries decreases in subsequent rows. The terms involving c_* in the upper diagonal are multiplied by N_O, because under the assumption of mean-field coupling, each open channel contributes equally to the elevation of the $[Ca^{2+}]$ above background at the model Ca^{2+} release site.

There are six parameters in this minimal model of a Ca^{2+} release site composed of mean-field and instantaneously coupled two-state Ca^{2+}-activated channels. These include the channel parameters themselves – the association (k^+) and dissociation (k^-) rate constants and the cooperativity of Ca^{2+} binding (η) – as well as the number of channels (N), the background $[Ca^{2+}]$ (c_∞), and the $[Ca^{2+}]$ increase contributed by each open channel (c_*). In principle, this last parameter can be calculated from the source amplitude of open channels using the well-studied equations for the buffered diffusion of intracellular Ca^{2+} [24,35]. We will refer to the parameter c_* as the release site "coupling strength", because it determines the degree to which open channels influence the rate of Ca^{2+}-mediated transitions of other channels at the same release site.

2.3. Stochastic attrition viewed as an absorption time on a terminating Markov chain

The tridiagonal generator matrix of Eq. (8) defines the Markov chain model of a Ca^{2+} release site composed of N two-state channels that is the focus of this work. Notice that no Ca^{2+}-dependent inactivation mechanism is included in the single channnel model (Eq. (2)) and, consequently, the state where all the channels at the release site are closed can be entered only via the process of stochastic attrition.

In order to analyze the dynamics of stochastic attrition in this model Ca^{2+} release site, we can view puff/spark duration as an absorption time on a terminating Markov chain that takes the form

$$Q_{attrit} = \left(\begin{array}{c|c} 0_{1\times 1} & \mathbf{0}_{1\times N} \\ \hline \mathbf{t}_{N\times 1} & T_{N\times N} \end{array}\right). \quad (9)$$

The $N+1 \times N+1$ generator matrix Q_{attrit} is identical to Q in Eq. (8) except that the first row is zeroed out, because it corresponds to the absorbing state where all channels are closed ($N_O = 0$). The $N \times N$ matrix T defines the dynamics of the transient states where $1 \le N_O \le N$ and is given by the lower right block of Q (see horizontal and vertical lines in Eq. (8)),

$$T = \begin{pmatrix} -k^- - (N-1)k^-(c_\infty + c_*)^\eta & (N-1)k^+(c_\infty + c_*)^\eta & & \diamond \\ & \ddots & & \\ & & (N-1)k^- & k^+(c_\infty + (N-1)c_*)^\eta \\ & & Nk^- & \diamond \end{pmatrix}. \tag{10}$$

The $N \times 1$ column vector $\boldsymbol{t} = (k^-, 0, \ldots, 0)^{\mathrm{T}}$ that gives the transition rates from transient to absorbing states has only one non-zero element, because the only way to enter the state $N_O = 0$ is via a transition from $N_O = 1$ to $N_O = 0$ at rate k^-. Similar to Q in Eq. (8), Q_{attrit} in Eq. (9) has row sums of zero; thus, we may write $\boldsymbol{t} = -T\boldsymbol{e}$ where $\boldsymbol{e}$ is a $N \times 1$ column vector of ones.

Eqs. (9) and (10) are the starting point for our analysis of the statistics of stochastic attrition. For example, the matrix T in Eq. (10) is invertible and the entries of the inverse of this matrix $[-T^{-1}]_{ij}$ denote the expected amount of time spent in state j before absorption given the initial state of the chain was $N_O = i$ [2,18]. Furthermore, if $\boldsymbol{\phi}$ is a vector of initial probabilities of the Ca^{2+} release site being in states $N_O = 1$ through $N_O = N$ we can write X_ϕ to indicate the random variable giving the time until absorption into state $N_O = 0$. The cumulative probability distribution for X_ϕ is

$$F_{X_\phi}(x) = 1 - \boldsymbol{\phi} \mathrm{e}^{x\mathrm{T}} \boldsymbol{e}. \tag{11}$$

where $\mathrm{e}^{x\mathrm{T}}$ is a matrix exponential and the probability density function of the random variable X_ϕ is given by

$$f_{X_\phi}(x) = \boldsymbol{\phi} \mathrm{e}^{xT} \boldsymbol{t}. \tag{12}$$

It can be shown be integrating Eq. (12) that the expected amount of time until absorption into state $N_O = 0$ given the initial probability distribution ϕ is

$$E[X_\phi] = \int_0^\infty x \boldsymbol{\phi} \mathrm{e}^{x\mathrm{T}} \mathbf{t} \, \mathrm{d}x = -\boldsymbol{\phi} T^{-1} \boldsymbol{e}, \tag{13}$$

which will evaluate to a positive scalar. Using Eq. (13), it can be shown that the entries of the $N \times 1$ vector,

$$\boldsymbol{h} = (h_i) = -T^{-1} \boldsymbol{e} \tag{14}$$

give the expected time until absorption (i.e., stochastic attrition) when the initial state of the release site is $N_O = i$. For example, if we define $\phi_1 = (1, 0, \ldots, 0)$ and $\phi_N = (0, \ldots, 0, 1)$, $h_1 = -\phi_1 T^{-1} \boldsymbol{e}$ and $h_N = -\phi_N T^{-1} \boldsymbol{e}$ give the expected amount of time until stochastic attrition occurs when the release site initially has one open channel or N open channels, respectively.

3. Results

3.1. Dynamics of stochastic attrition

Fig. 2A shows a stochastic trajectory of a Markov chain model of a moderately sized Ca^{2+} release site composed of 19 two-state channels under the assumptions of mean-field and instantaneous coupling (Eq. (7)). Consistent with previous work in which an identical number of channels were arranged in a hexagonal lattice (without making the assumption of mean-field coupling), stochastic Ca^{2+} excitability is observed in Fig. 2A in spite of the fact that there is no Ca^{2+} inactivation mechanism in the single-channel model (Eq. (2)). Indeed, the single-channel model includes Ca^{2+} activation but not Ca^{2+} inactivation and, consequently, the termination of these simulated puffs/sparks must be attributed to the phenomenon of stochastic attrition.

Fig. 2B shows the three largest amplitude stochastic Ca^{2+} release events of Fig. 2A – in each case the number of open channels is transiently greater than five ($N_O > 5$). The *filled circles* of Fig. 2B illustrate that the puff/spark duration (or equivalently, the time until stochastic attrition) is a random variable (X_ϕ) whose distribution depends on the number of open channels chosen for the initial state. The three events

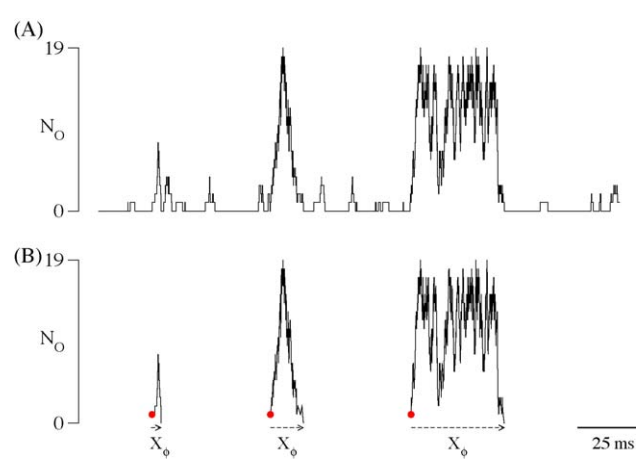

Fig. 2. (A) Markov chain model of a Ca^{2+} release site with 19 two-state channels exhibiting stochastic Ca^{2+} excitability. The single-channel model (Eq. (2)) does not include Ca^{2+} inactivation and, consequently, the simulated Ca^{2+} puffs/sparks are terminating via stochastic attrition. Parameters used: $N = 19$, $\eta = 2$, $c_\infty = 0.05\ \mu\mathrm{M}$, $c_* = 0.06\ \mu\mathrm{M}$, $k^+ = 1.5\ \mu\mathrm{M}^{-2}\ \mathrm{ms}^{-1}$, $k^- = 0.5\ \mathrm{ms}^{-1}$. (B) Three large amplitude puff/spark events from (A) are reproduced to show diagramatically that the time until stochastic attrition occurs is a random variable (X_ϕ) parameterized by the probability distribution over initial states (ϕ). Here $\boldsymbol{\phi} = \phi_1 = (1, 0, \ldots, 0)$ and the initial state is $N_O = 1$ (*filled circles*).

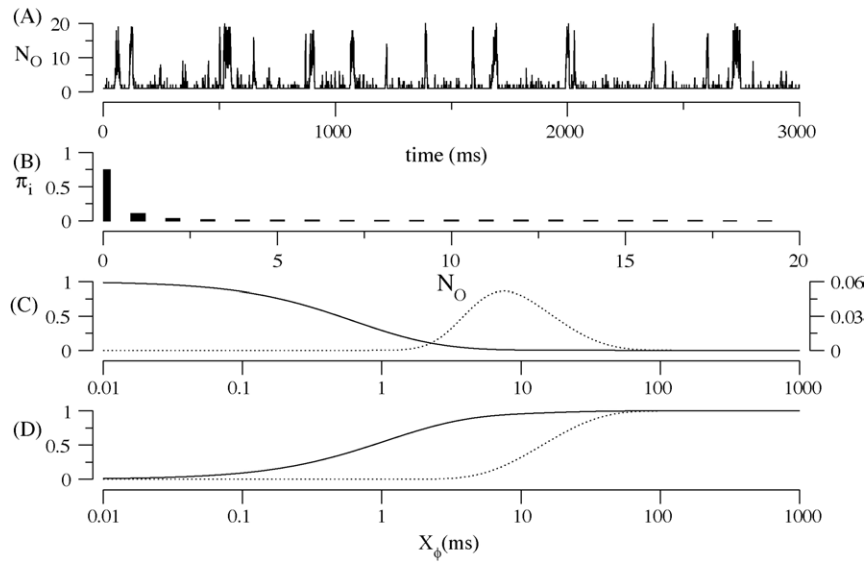

Fig. 3. (A) Ca^{2+} release site simulations with 19 two-state channels exhibiting Ca^{2+} puffs/sparks that terminate via stochastic attrition. Total time is 3 s. Parameters as in Fig. 2 (B) Stationary probability distribution of the number of open channels: $\boldsymbol{\pi} = (\pi_i)$ where $0 \le i \le N$. (C) Probability density function of the time until stochastic attrition (X_ϕ) given by Eq. (12) with an initial state of one channel open (*solid line*) or $N = 19$ channels open (*dotted line,* alternate *y*-axis). (D) The corresponding cumulative distribution function for X_ϕ given by Eq. (11).

shown use $\boldsymbol{\phi} = \phi_1 = (1, 0, \ldots, 0)$ – corresponding to an initial state of $N_O = 1$ – and have durations of approximately 4, 15, and 42 ms, respectively. Fig. 2A also shows many smaller amplitude events (i.e., blip or quarks) for which the time until stochastic attrition can be several milliseconds or less.

Fig. 3A shows a 3-sec simulation of a Ca^{2+} release site exhibiting multiple large amplitude puff/spark events that terminate through the process of stochastic attrition (parameters as Fig. 2). As a first step in characterizing the stochastic gating of this Ca^{2+} release site, Fig. 3B shows the limiting probability distribution for the number of open channels (N_O) that is obtained in a long simulation such as that in Fig. 3A. Because the Markov chain model has a finite number of states and is irreducible, this limiting probability distribution is equivalent to the stationary probability distribution $\boldsymbol{\pi} = (\pi_0, \pi_1, \ldots, \pi_N)$ solving $\pi Q = 0$ (using the generator matrix of Eq. (8)) subject to conservation of probability ($\boldsymbol{\pi}\mathbf{e} = 1$) [39]. This stationary probability distribution ($\boldsymbol{\pi}$) plotted in Fig. 3B shows that the release site is most often found in the state where all channels are closed ($N_O = 0$, $\pi_0 = 0.75$). Indeed, the sum of π_0 to π_4 is 0.91 indicating that when the trajectories of Fig. 3A are sampled at random the probability of observing more than four open channels is less than 10%. Nevertheless, the transient opening of channels at the release site is a notable aspect of the dynamics of stochastic attrition in Fig. 3A.

In order to further analyze the statistics of stochastic attrition, the *solid line* of Fig. 3C shows the probability density function for the puff/spark duration (that is, the time until absorption into state $N_O = 0$) when the initial state is one open channel ($N_O = 1$). Using Eqs. (10) and (14), we find that this distribution has mean of $h_1 = 4.7$ ms consistent with the semilogarithmic plot of $f_{X_\phi}(x)$ (Eq. (12)). The *dotted line* of Fig. 3C shows the probability density for the puff/spark duration when all the channels of the release site are initially open ($N_O = N = 19$); in this case, the expected time until absorption is 36 ms. This is consistent with our intuition that that a fully activated release site should take longer on average to extinguish than a minimally activated release site. As shown in Table 1, the expected puff/spark duration is a monotonically increasing function of the initial number of open channels.

Table 1
Expected puff/spark duration

$N_O^{init} = 1$	h_i (ms)	$N_O^{init} = 1$	h_i (ms)	$N_O^{init} = 1$	h_i (ms)	$N_O^{init} = 1$	h_i (ms)
1	4.7	6	24.7	11	33.9	16	36.0
2	8.8	7	27.6	12	34.6	17	36.2
3	13.1	8	29.9	13	35.1	18	36.3
4	17.3	9	31.6	14	35.5	19	36.4
5	21.3	10	32.9	15	35.8		

The expected puff/spark duration (that is, the time until absorption into the state $N_O = 0$) is a monotonically function of the initial number of open channels $N_O = i$ (Eqs. (10) and (14)). Parameters as Fig. 3A.

3.2. The dependence of stochastic attrition on coupling strength and the cooperativity of Ca^{2+} binding

While many choices of Ca^{2+} release site parameters do not lead to stochastic Ca^{2+} excitability in which the termination of Ca^{2+} puffs/sparks occurs via stochastic attrition, the specific parameters used to generate Fig. 3A are certainly not unique. In this section, we will explore how the cooperativity of Ca^{2+} binding (η) and the coupling strength (c_*) determine the significance of stochastic attrition as a puff/spark termination mechanism.

To facilitate this parameter study we introduce a response measure whose value correlates well with the presence of puff/spark events in stochastic Ca^{2+} release site simulations – the so-called puff/spark *Score*. First, we define the fraction of open channels in a release site as $f_O = N_O/N$, that is f_O is a random function of time proportional to Fig. 3A that takes values between 0 and 1. The puff/spark *Score* is then simply defined as the index of dispersion of the fraction of open channels [24], that is,

$$Score = \frac{\mathrm{Var}[f_O]}{\mathrm{E}[f_O]} = \frac{1}{N}\frac{\mathrm{Var}[N_O]}{\mathrm{E}[N_O]}. \quad (15)$$

This response measure takes values between 0 and 1, with values greater than approximately 0.3 corresponding to the presence of robust Ca^{2+} puffs/sparks.

Fig. 4A, C, and E show three stochastic Ca^{2+} release site simulations demonstrating that an elevated *Score* corresponds to the presence of Ca^{2+} puffs/sparks. The parameters used are identical to Figs. 2 and 3 except that the coupling strength takes values of $c_* = 0.04$, 0.06, and 0.08 μM. In Fig. 4A, the coupling strength is insufficient to allow generation of Ca^{2+} puff/spark events and the *Score* is a comparatively low value of 0.09. In Fig. 4E, the *Score* is also quite low (*Score* = 0.04) because the coupling strength is *too strong* for puff/spark events to terminate via stochastic attrition. In Fig. 4C, the coupling strength of $c_* = 0.06$ μM leads to robust Ca^{2+} puffs/sparks and a comparatively large *Score* of 0.43. Fig. 4B, D, and F show the stationary probability distributions for the number of open channels as the coupling strength is increased. The rightward shifts in these distributions correspond to an increase in the expected number of open channels ($\mathrm{E}[N_O]$) as the coupling strength (c_*) is increased (compare Fig. 4D and E).

Fig. 5 summarizes the results of many simulations such as Fig. 4 by plotting the *Score* for 19 channel Ca^{2+} release site simulations as a function of the coupling strength (c_*). The *thick solid line* of Fig. 5 shows that when the cooperativity of Ca^{2+} binding is $\eta = 2$ the puff/spark *Score* first increases and then decreases as a function of the coupling strength c_*. The *filled square, circle*, and *triangle* correspond to the simulations presented in Fig. 4A, C, and E, respectively. Because simulations such as those in Fig. 4 indicate that a *Score* of 0.3 or more corresponds to robust puffs or sparks, we conclude that the range of coupling strengths leading to significant stochastic Ca^{2+} excitability in this release site composed of 19 two-state channels is approximately $c_* = 0.056$–0.070 μM.

To determine the extent to which the phenomenon of stochastic attrition depends on the cooperativity of Ca^{2+} binding (η) in the two state model (Eq. (2)), Fig. 5 also shows the *Score* as a function of the coupling strength (c_*) for release

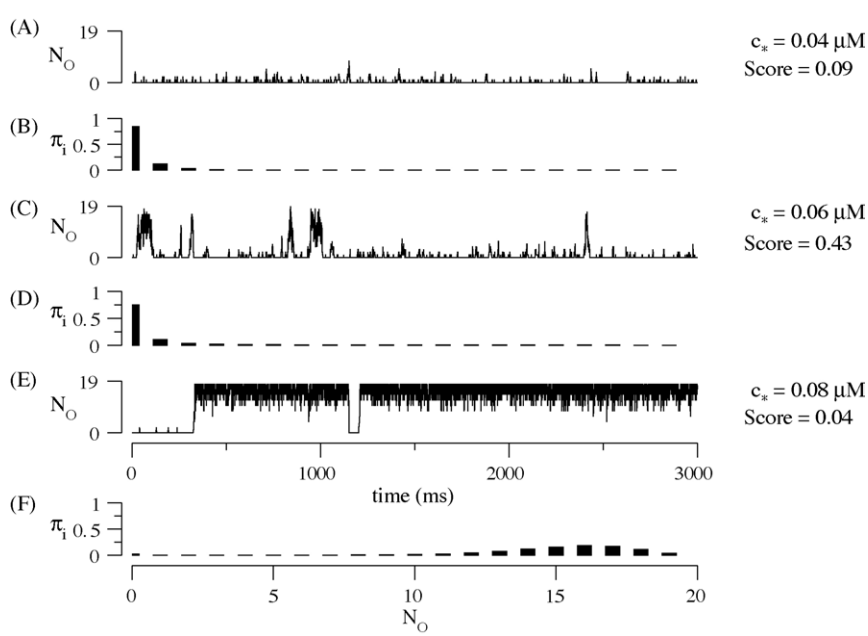

Fig. 4. (A, C, E) Ca^{2+} release site simulations with 19 two-state channels using different values of the coupling strength: $c_* = 0.04$, 0.06, and 0.08 μM, respectively. Other parameters as in Fig. 3. Only the intermediate value of 0.06 μM (A) leads to robust puff/spark events. (B, D, F) The stationary probability distributions for A, C, and E, respectively: $\boldsymbol{\pi} = (\pi_i)$ with $0 \le i \le N$.

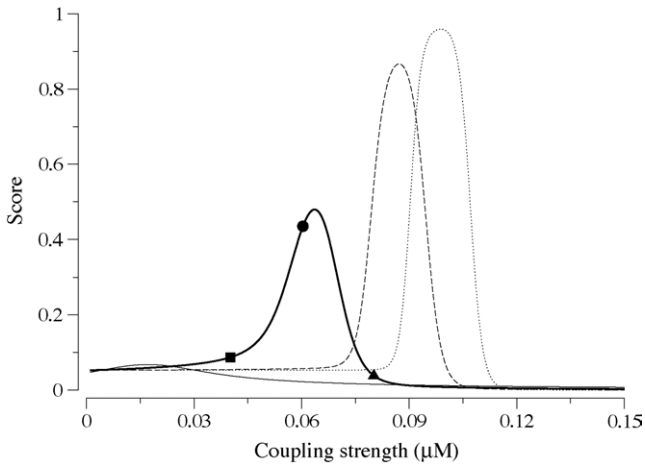

Fig. 5. The Ca^{2+} puff/spark *Score* as a function of the coupling strength c_* and the cooperativity of Ca^{2+} binding for $\eta = 1$ (*thin solid line*), 2 (*thick solid line*), $\eta = 3$ (*dashed line*), and $\eta = 4$ (*dotted line*). Other parameters as in Fig. 3. The *filled square, circle*, and *triangle* correspond to Fig. 4A, C, and E, respectively.

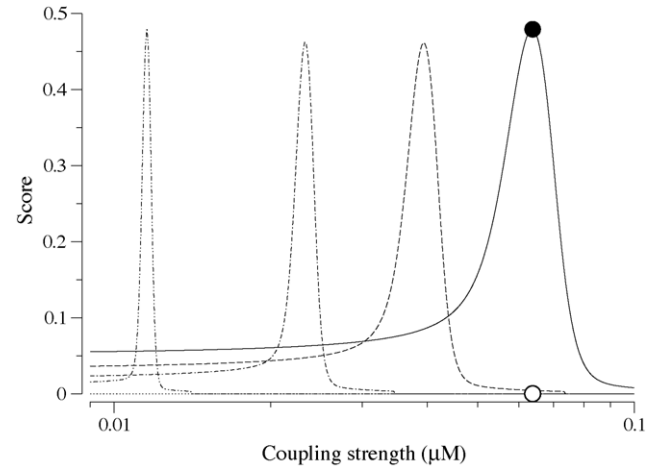

Fig. 6. The Ca^{2+} puff/spark *Score* as a function of the coupling strength (c_*) when the number of two-state Ca^{2+}-activated channels is $N = 19$ (*solid line*), $N = 30$ (*dashed line*), $N = 50$ (*dot–dash–dashed line*), $N = 100$ (*dot–dot dashed line*), and $N = 150$ (*dotted line*). Other parameters as in Fig. 3.

sites using $\eta = 1$, 3, and 4. So long as the cooperativity of Ca^{2+} binding is greater than or equal to 2 ($\eta \geq 2$) we find that a range of coupling strengths give rise to spontaneous Ca^{2+} puffs/sparks with *Scores* greater than 0.3. We also find that the maximum possible *Score* increases as the cooperativity of Ca^{2+} binding increases; in the case of $\eta = 4$, the optimal *Score* is nearly 1. However, when the cooperativity of Ca^{2+} binding is $\eta = 1$, robust Ca^{2+} puffs/sparks terminated by stochastic attrition are not observed regardless of coupling strength (*thin solid line*).

3.3. Stochastic attrition can occur for release sites composed of many channels

In Sections 3.1 and 3.2, we focused on the stochastic gating of Ca^{2+} release sites composed of 19 two-state channels that are activated, but not inactivated, by Ca^{2+}. In order to determine how the dynamics of stochastic attrition depend on the number of such two-state channels at a Ca^{2+} release site, Fig. 6 shows the *Score* as a function of coupling strength for release sites composed of 19, 30, 50, 100 and 150 channels modeled using generator matrices similar to Eq. (10) but of larger size. Because a *Score* of greater than 0.3 corresponds to a Ca^{2+} release site simulation with robust puffs/sparks, Fig. 6 demonstrates that for each value of N studied there exists a range of coupling strengths (c_*) that gives rise to puffs/sparks terminated by stochastic attrition, though the range of coupling strengths leading to stochastic Ca^{2+} excitability narrows as N increases. The *filled* and *open* circles of Fig. 6 show that when the coupling strength is fixed, increasing the number of two-state Ca^{2+} activated channels from $N = 19$ to 30 or more may lead to a tonically active release site. However, Ca^{2+} release sites composed of large numbers of instantaneously coupled two-state channels (up to 150 shown here) are capable of generating puffs/sparks terminating by stochastic attrition so long as the coupling strength (c_*) is appropriately chosen.

Interestingly, Fig. 6 shows that the optimal value coupling strength – that is the value of c_* leading to the highest *Score* – *decreases* as the number of channels in the release site increases (compare location of peaks). In fact, for fixed channel parameters (k^+, k^-, η), the product of the optimal coupling strength (c_*^{opt}) and the number of channels at the release site is nearly invariant. More precisely, using the optimal coupling strength (c_*^{opt}) value for a given N, the value of $\tilde{c}_*^{opt}$ that will produce the maximum *Score* for any other $\tilde{N}$ of interest is given by

$$\tilde{c}_*^{opt} = \frac{c_*^{opt}(N-1)}{\tilde{N}-1} \tag{16}$$

Fig. 7 confirms this relationship by plotting the optimal coupling strength (c_*^{opt}, *filled circles*) for Ca^{2+} release sites with a range of sizes (N). The *dotted line* in Fig. 7 is a plot of optimal coupling strength $\tilde{c}_*^{opt}$ as a function of $\tilde{N}$ as predicted by Eq. (16) with $c_*^{opt} = 0.0637\,\mu M$ and $N = 19$. The agreement between the *filled circles* and *dashed line* of Fig. 7 confirms that as the number of channels in a Ca^{2+} release site increases, the optimal coupling strength decreases in a matter well-approximated by Eq. (16).

It is important to note that the optimal *Scores* presented in Fig. 7 are all in the range 0.461–0.488 as N increases from 19 to 250. Thus, Fig. 7 demonstrates that Ca^{2+} release sites with very large numbers of channels are still capable of exhibiting puffs/sparks that are terminated by stochastic attrition when the coupling strength (c_*) is optimally chosen. To clarify this point, Fig. 8A–D shows representative stochastic gating of Ca^{2+} release sites composed of $N = 19$, 50, 100, and 150 two-state Ca^{2+}-activated channels, respectively (corresponding to three peaks in Fig. 6 and the *open circles* in Fig. 7. In each

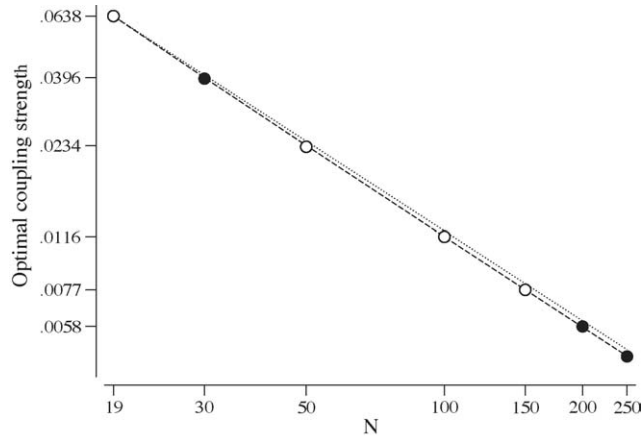

Fig. 7. The optimal coupling strength (c_*^{opt}) – that is, the value of c_* leading to maximum puff/spark *Score* – is a decreasing function of the number of channels (N) in Ca^{2+} release sites composed of coupled two-state channels. *Filled* and *open circles* summarize results from calculations similar to Fig. 4. The *dashed line* shows the relationship predicted by Eq. (16) where $N = 19$ and $c_*^{opt} = 0.0637\ \mu M$ while the *dotted line* is $\tilde{c}_*^{opt} = c_*^{opt} N/\tilde{N}$.

panel, the cooperativity of Ca^{2+} binding is $\eta = 2$ and the coupling strength leading to optimal *Score* – found using Fig. 7 or Eq. (16) – leads to stochastic Ca^{2+} excitability in spite of the fact that there is no Ca^{2+} inactivation in the single-channel model (Eq. (2)). The association and dissociation rate constants (k^+ and k^-) used in Fig. 8B–D were chosen so that the expected time until stochastic attrition from state $N_O = N$ to $N_O = 0$ is 63.2 ms in each panel and the dissociation constant ($K^\eta = k^-/k^+ = 0.33\ \mu M^\eta$) remains fixed; the background $[Ca^{2+}]$ is also fixed at $c_\infty = 0.05\ \mu M$. Fig. 8 shows that when release sites are composed of a large number of channels (N), the parameters of the single-channel model (k^+, k^-, and η) can be chosen so that robust Ca^{2+} puffs/sparks are terminated via stochastic attrition. Interestingly, when N is large the Ca^{2+} puffs/sparks appear more "boxy" (compare Fig. 8B and D), indicating that the stationary probability distribution is distinct in Fig. 8A–D. Specifically, when N is large it is unlikely that the Ca^{2+} release site will be found with the fraction of open channels ($f_O = N_O/N$) in the range 0.1–0.2.

3.4. The expected time until stochastic attrition

The previous section explored how the ability of stochastic attrition to terminate Ca^{2+} puffs and sparks depends on the number of channels at a release site (N) and how strongly they are coupled (c_*). These calculations include Ca^{2+}-regulation and cooperative Ca^{2+} binding and, consequently, the expected time for stochastic attrition to occur can be much shorter (or much longer) than that predicted by the back-of-the-envelope calculation that assumes independent and uncoupled channels (Eq. (1)). In this section, we derive an analytical formula analogous to Eq. (1) for the expected time until stochastic attrition in a release site composed of N instantaneously and mean-field coupled two-state Ca^{2+}-activated channels (Eq. (2)).

As discussed in Section 2.2, there are six parameters in this minimal model of a release site composed of two-state Ca^{2+}-activated channels. These include the channel parameters

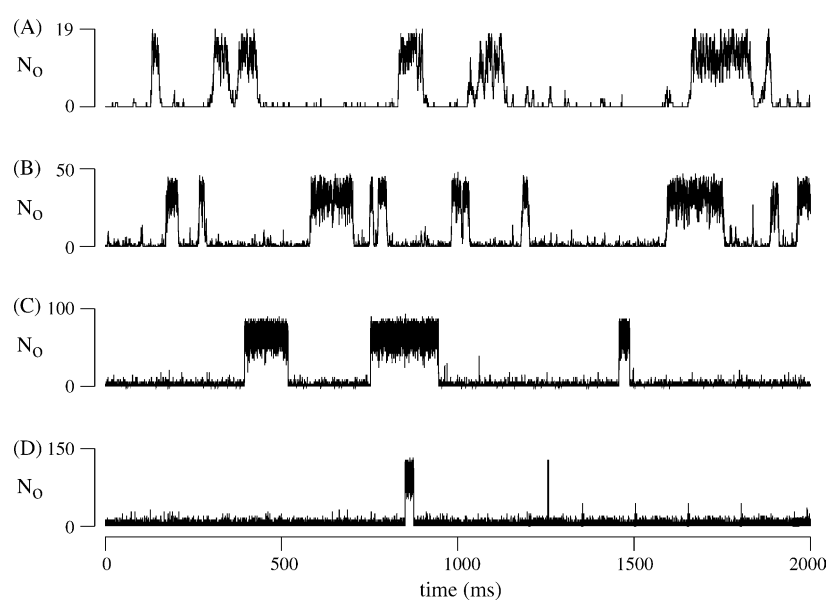

Fig. 8. (A–D) Ca^{2+} release site simulations with $N = 19$, 50, 100 and 150 two-state Ca^{2+}-activated channels using the optimal coupling strength-the value of c_* leading to the maximum possible *Score* (0.0637, 0.0234, 0.0116, and 0.0077 μM, respectively). Association and dissociation rate constants ($k^\pm$) are chosen so that the time to absorption from state $N_O = N$ to $N_O = 0$ is 63.2 ms regardless of N. These rate constants are given by $k^- = k^+K^\eta$ and $k^+ = 1.5$, 6.94, 65.85, and 651.81 $\mu M^{-\eta} ms^{-1}$, respectively, so that dissociation constant K is fixed ($K^\eta = 0.33\ \mu M^\eta$). The cooperativity of Ca^{2+} binding is $\eta = 2$ and the background $[Ca^{2+}]$ is $c_\infty = 0.05\ \mu M$.

themselves – the association (k^+) and dissociation (k^-) rate constants and the cooperativity of Ca^{2+} binding (η) – as well as the number of channels (N), the background [Ca^{2+}] (c_∞), and the [Ca^{2+}] increase contributed by each open channel (c_*). To calculate the expected time until stochastic attrition, it is helpful to measure concentration in units of the dissociation constant for Ca^{2+} binding to the two-state channel (K) and measure time in units of the reciprocal of the dissociation rate constant (k^-). Thus, we write

$$\hat{c}_* = \frac{c_*}{K}, \quad \hat{c}_\infty = \frac{c_\infty}{K}, \quad \hat{Q} = Qk^- \tag{17}$$

and substitute these expressions into Eq. (8) to find a dimensionless generator matrix for the Ca^{2+} release site composed of coupled two-state channels,

$$\hat{Q} = \begin{pmatrix} & N\hat{c}_\infty^\eta & & & & \\ 1 & \diamond & (N-1)(\hat{c}_\infty + \hat{c}_*)^\eta & & & \\ & & \diamond & (N-2)(\hat{c}_\infty + 2\hat{c}_*)^\eta & & \\ & & & \ddots & & \\ & & & (N-1) & \diamond & (\hat{c}_\infty(N-1)\hat{c}_*)^\eta \\ & & & & N & \diamond \end{pmatrix}. \tag{18}$$

Notice that the six parameters of the original dimensional generator matrix (k^+, k^-, c_∞, c_*, N, and η in Eq. (8) correspond to four dimensionless parameters ($\hat{c}_\infty$, $\hat{c}_*$, N, and η in Eq. (18)). When the dimensionless versions of $\hat{Q}_{\text{attrit}} = Q_{\text{attrit}}k^-$ and $\hat{T} = Tk^-$ are defined as in Eq. (9), the dimensionless hitting time vector $\hat{\boldsymbol{h}} = \boldsymbol{h}k^-$ is given by $\hat{\boldsymbol{h}} = -\hat{T}^{-1}\boldsymbol{e}$. Beginning with Eq. (18), Appendix B shows that the expected time until absorption into state $N_O = 0$ given an initial state of $N_O = 1$ (that is, h_1) is given by

$$\tau_{\text{attrit}} = \frac{1}{k_{\text{attrit}}} = \frac{1}{k_-}\left\{1 + \sum_{i=1}^{N-1}\left[\frac{(N-1)!}{(i+1)!(N-1-i)!} \times \prod_{j=1}^{i}\left(\frac{c_\infty + jc_*}{k}\right)^\eta\right]\right\} \tag{19}$$

where $K^\eta = k^-/k^+$ as defined above. This expression is a generalization of Eq. (1) that gives the expected time until stochastic attrition occurs for a release site composed of N coupled two-state Ca^{2+}-activated channels.

The non-dimensionalization presented above allows a full exploration of the contribution of stochastic attrition to the termination of Ca^{2+} puffs/sparks. For example, Fig. 9A shows the Ca^{2+} puff/spark *Score* as a function of the dimensionless coupling strength ($\hat{c}_*$) and dimensionless background [Ca^{2+}] ($\hat{c}_\infty$) for a release site composed of 19 two-state Ca^{2+}-activated channels with cooperativity of Ca^{2+} binding $\eta = 2$. Fig. 9A shows that for any dimensionless background [Ca^{2+}] ($\hat{c}_\infty = c_\infty/K$) less than approximately 0.1, a dimensionless coupling strength of approximately $\hat{c}_* = c_*/K = 0.1$

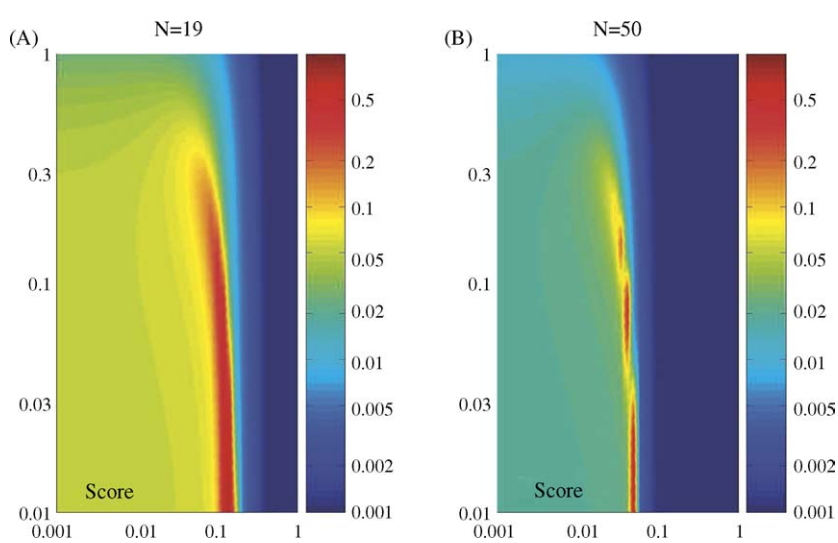

Fig. 9. (A) The Ca^{2+} puff/spark *Score* plotted in pseudocolor as a function of the dimensionless coupling strength ($\hat{c}_*$) and dimensionless background [Ca^{2+}] ($\hat{c}_\infty$) for a release site composed of coupled two-state Ca^{2+}-activated channels with cooperativity of Ca^{2+} binding $\eta = 2$. The number of channels is $N = 19$ (A) and 50 (B), respectively.

leads to a high *Score*. As the dimensionless background $[Ca^{2+}]$ increases from 0.1 to 0.3, the optimal dimensionless coupling strength decreases slightly; when the dimensionless background $[Ca^{2+}]$ is greater than approximately 0.3, there is no coupling strength leading to a high puff/spark *Score*. Fig. 9B shows that for Ca^{2+} release sites composed of $N = 50$ coupled two-state channels the range of dimensionless coupling strengths leading to a high *Score* narrows and the maximum dimensionless background $[Ca^{2+}]$ that permits Ca^{2+} puffs/sparks terminated by stochastic attrition decreases slightly. Comparing Fig. 9A and B for low dimensionless background $[Ca^{2+}]$ (e.g., $\hat{c}_\infty = 0.01$), we see that the optimal dimensionless coupling strength for $N = 50$ channels is less than the optimal dimensionless coupling strength for $N = 19$ channels (consistent with Eq. (16) and Fig. 6).

4. Discussion

In this paper, we investigate the statistical properties of stochastic attrition viewed as an absorption time on a terminating Markov chain representing Ca^{2+} release sites composed of N two-state Ca^{2+}-activated channels. In release sites composed of comparatively small number of channels (e.g., $N = 19$ in Fig. 3), Monte Carlo simulation indicates that robust Ca^{2+} puffs and sparks can be observed in spite of the fact that Ca^{2+} inactivation is not present in the single-channel model (Eq. (2)). Several parameter studies involving a response measure referred to as the Ca^{2+} puff/spark *Score* show that stochastic attrition is sufficient as a termination mechanism for Ca^{2+} puffs and sparks so long as cooperative Ca^{2+} binding is included in the single-channel model ($\eta \geq 2$).

Interestingly, when simulations are performed with large numbers of two-state Ca^{2+}-activated channels (up to $N = 250$ in Fig. 7 and $N = 150$ in Fig. 8), robust Ca^{2+} puffs/sparks terminated by stochastic attrition are observed so long as the coupling strength (c_*) and channel kinetics (k^+ and k^-) are chosen appropriately. At first glance, this result appears to be in disagreement with a back-of-the-envelope calculation (Eq. (1)) indicating that the time constant of stochastic attrition is an exponential function of the number of channels in a Ca^{2+} release site. However, Eq. (1) is derived under the unphysiological assumption that a release site is composed of *uncoupled and independent* channels. Conversely, this analysis begins with a minimal representation of the influence of open Ca^{2+} channels on the Ca^{2+}-regulation and subsequent stochastic gating of Ca^{2+} release sites. With this addition of this physiological realism, we find that stochastic attrition is not so easily eliminated as a potential Ca^{2+} puff/spark termination mechanism.

Our results indicate that the significance of stochastic attrition as a Ca^{2+} puff/spark termination mechanism depends on the coupling strength (c_*), the background $[Ca^{2+}]$ (c_∞), and the dissociation constant for Ca^{2+} binding to a two-state Ca^{2+}-activated channel (K). Analysis of a non-dimensionalized generator matrix for a collection of N two-state Ca^{2+}-activated channels (Eq. (17)) shows that so long as the ratio ($\hat{c}_\infty = c_\infty/K$) is small enough, there is always a range of dimensionless coupling strengths ($\hat{c}_* = c_*/K$) leading to robust Ca^{2+} puffs/sparks terminated by stochastic attrition. This non-dimensionalization also facilitates the derivation of an analytical formula for the time until stochastic attrition (Eq. (19)) that generalizes Eq. (1) to the case of coupled channels. Indeed, when the coupling strength is set to zero ($c_* = 0$), Eq. (19) reduces to Eq. (1).

It is important to note that we observe stochastic attrition serving as a Ca^{2+} puff/spark termination mechanism in situations where the stochastic attrition time constant for uncoupled channels (Eq. (1)) suggests that termination by stochastic attrition was highly unlikely. For example, in the simulation presented in Fig. 8D involving 150 coupled channels, the expected value for the time until stochastic attrition is 63.2 ms (Eq. (14)). However, the mean open time of the two-state channels is $\tau_O = 1/k^- = 0.005$ ms and the open probability – equivalent to the steady-state open fraction of channels – is $f_O = p_O = 0.1$. Substitution of these values into Eq. (1) suggests a stochastic attrition time constant of approximately 2.4 h, values that are not consistent with Fig. 8D. Thus, it is clear that by neglecting coupled gating Eq. (1) may overestimate the expected time until stochastic attrition occurs.

As mentioned above, we find that as long as the dimensionless background $[Ca^{2+}]$ ($\hat{c}_\infty = c_\infty/K$) is small enough, there is always a range of dimensionless coupling strengths ($\hat{c}_* = c_*/K$) leading to robust Ca^{2+} puffs/sparks terminated by stochastic attrition. It is important to note that although the coupling strength is a monotonic function of the source amplitude of open channels in a Ca^{2+} release site [24], the dimensionless coupling strength c_* is also determined by the dissociation constant for Ca^{2+} binding the channels (K). This means that the small optimal dimensionless coupling strengths observed for large N do not imply that unphysiologically small single-channel conductances are required for Ca^{2+} sparks/puffs to be terminated by stochastic attrition.

On the other hand, several important caveats are required so as not to misinterpret these simulations of Ca^{2+} puffs/sparks terminated by stochastic attrition. First, we consistently observe an optimal coupling strength leading to robust Ca^{2+} puffs/sparks terminating by stochastic attrition, but the range of values around this maximum becomes narrow with large N. For example, for low dimensionless background $[Ca^{2+}]$, the range of coupling strengths leading to a *Score* ≥ 0.3 is approximately four times the size when $N = 19$ channels than when $N = 50$ channels (cf. Fig. 9).

Secondly, it is important to recognize that the assumptions of mean-field and instantaneous coupling are limitations of the analysis of stochastic attrition presented here; and yet, we hasten to add, these assumptions are much to be preferred over the assumption of independent and uncoupled channels that has appeared in previous work (Eq. (1)). When instantaneously coupled channels are assigned specific spatial locations, the dynamics of stochastic Ca^{2+} excitability are often similar to simulations utilizing a mean-field approxima-

tion [24]. On the other hand, in some cases the dynamics of instantaneously coupled Ca^{2+} release sites depends on the precise location of channels, even when the average channel density at a Ca^{2+} release site is unchanged [23]. For example, the dynamics of Ca^{2+} release sites composed of single-channel models that include fast Ca^{2+} activation but no slow Ca^{2+} inactivation (Eq. (2)) tend to be more sensitive to channel position than release sites composed of single-channel models that include both Ca^{2+} activation and Ca^{2+} inactivation – e.g., the four-state type 1-like IP_3R model presented in [24].

Similarly, the assumption of instantaneous coupling is a limitation of the present study. When two-state Ca^{2+}-activated channels are coupled via a time-dependent Ca^{2+} domain as in [21], the time constant for Ca^{2+} domain formation and collapse can have a strong effect on both the generation and termination of Ca^{2+} puffs/sparks. For example, if the domain $[Ca^{2+}]$ does not increase fast enough in response to a single-channel opening, Ca^{2+} blips and quarks are unlikely to trigger puffs and sparks. Similarly, if the domain $[Ca^{2+}]$ does not drop quickly in response to the spontaneous closing of channels, residual Ca^{2+} from previous channel openings may prohibit termination of Ca^{2+} release events via stochastic attrition [43].

Thirdly, we observed for coupled two-state Ca^{2+} activated channels leading to robust Ca^{2+} puffs/sparks only when the cooperativity of Ca^{2+} binding was 2 or more. More biophysically realistic single-channel models also exhibit cooperative Ca^{2+}-regulation through the gating of independent subunits, some number of which must be permissive for the channels to be open. For example, the transition state diagram

$$C_1 \underset{k^-}{\overset{2k^+c}{\rightleftharpoons}} C_2 \underset{2k^-}{\overset{k^+c}{\rightleftharpoons}} O,$$

represents a two-subunit channel that is open only when both subunits are permissive. When such Ca^{2+}-regulated channel models are instantaneously coupled, we have repeatedly observed that cooperative Ca^{2+} regulation due to the sequential binding of multiple Ca^{2+} ions is able to substitute for the instantaneous binding of multiple Ca^{2+} ions implied by Eq. (2) [24]. This sets to rest the concern that the simplicity of the two-state Ca^{2+}-activated channel model that is the focus of this paper somehow makes it more likely for stochastic attrition to occur. In future work, we hope to more fully explore the relationship between single-channel kinetics and stochastic Ca^{2+} excitability using more complex and realistic single-channel models and, when possible, relaxing the assumptions of mean-field and instantaneous coupling.

Finally, it is important to note that the question of whether stochastic attrition is a theoretical possibility is model and parameter-dependent and must be determined on a case-by-case basis. The observation that Ca^{2+} inactivation is *not* a requirement for puff- and spark-like dynamics in the simulations presented here is intriguing, because Ca^{2+} inactivation and the 'bell-shaped' curve relating $[Ca^{2+}]$ to channel open probability does not apply to all IP_3R and RyR isoforms [15,28,8]. However, we should remind ourselves that whether or not stochastic attrition, Ca^{2+} inactivation, adaptation, dissociation of co-agonist, or other mechanism determines Ca^{2+} puff or spark duration in any particular cell type is an empirical question [31,20]. But in spite of these caveats, it seems reasonable to interpret the robust Ca^{2+} puffs/sparks observed in these simulations of coupled two-state channels as a demonstration that the phenomenon of stochastic attrition may contribute more significantly to the termination of stochastic Ca^{2+} release events than previously supposed.

Appendix A. Stochastic attrition time constant for independently gating channels

In order to quantify the possible contribution of stochastic attrition to the termination of puffs and sparks, investigators have roughly estimated the rate of termination events (k_{attrit}) in a cluster of N uncoupled and independent channels toggling between open and closed states with mean open time τ_O and open probability p_O [36,37]. Assuming the channels are not only identical but also independent, the steady-state number of open channels (N_O) is binomially distributed, that is,

$$P\{N_O = n\} = \binom{N}{n} (1 - p_O)^{N-n} p_O^n.$$

where $0 \le n \le N$. Conditioning the above distribution on $N_O \neq 0$ gives

$$P\{N_O = n | N_O \neq 0\} = \frac{\binom{N}{n} (1 - p_O)^{N-n} p_O^n}{1 - (1 - p_O)^N}.$$

where $0 \le n \le N$. The rate of extinction events (that is, $N_O = 1$ to $N_O = 0$ transitions) is obtained by multiplying $P\{N_O = n | N_O = 0\}$ by the $N_O = 1 \to 0$ transition rate constant ($k_- = 1/\tau_O$),

$$k_{\text{attrit}} = k_- \frac{N(1 - p_O)^{N-1} p_O}{1 - (1 - p_O)^N}.$$

This expression is then inverted to give Eq. (1), the time constant for stochastic attrition for N uncoupled and independently gating two-state channels.

Appendix B. Expected time until stochastic attrition for coupled two-state channels

The expected time until stochastic attrition for coupled two-state channels can be derived using Hill's diagrammatic method for calculating the mean absorption time on a terminating Markov chain [16]. Beginning with the transition-state diagram for N coupled two-state channels (Fig. 10A), a modified transition-state diagram (Fig. 10B) is constructed by eliminating the absorbing state ($N_O = 0$). Next, any transitions leading to the absorbing state (here q_{10} is the only one)

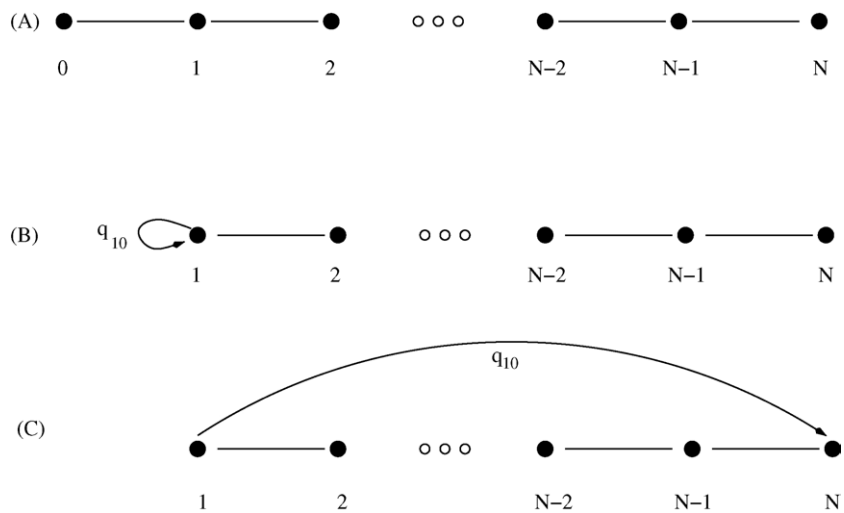

Fig. 10. (A): The topology of the transition-state diagram for N coupled two-state channels (Eq. (7)). *Solid lines* represent bidirectional transitions between states ($0 \le N_O \le N$). The transition rate from state $N_O = i$ to state $N_O = j$ is given by q_{ij} in Eq. (8). (B, C): Modified transition-state diagrams used to calculate the expected time until absorption into state $N_O = 0$ when the initial state is $N_O = 1$ and $N_O = N$, respectively. A unidirectional transition from the absorbing state ($N_O = 0$) to the initial state ($N_O = 1$ in B and $N_O = N$ in C) occurs at rate q_{10}.

are redrawn so that the destination state is the initial state of the Markov chain (here $N_O = 1$). Thus, the modified transition diagram of Fig. 10B corresponds to a Markov chain where, upon absorption into state $N_O = 0$, a new process immediately begins in state $N_O = 1$. Fig. 10C shows the modified transition-state diagram that results when state $N_O = N$ is the initial state of the Markov chain.

The stationary distribution of the modified transition diagram can be found by considering the transition rates directed toward each of the N states in Fig. 10B. After non-dimensionalization, these rates are

$$\hat{q}_{n,n-1} = n \quad \text{and} \quad \hat{q}_{n,n+1} = (N-n)\hat{c}_n = (N-n)(\hat{c}_\infty + n\hat{c}_*)$$

where $1 \le n \le N$ (recall that the state where $N_O = 0$ has been removed). We indicate the transition rates directed toward state n as z_n and write,

$$z_n = \frac{N!}{n!} \cdot \frac{N!}{(N-n)!} \prod_{i=1}^{n-1} \hat{c}_i$$

where the first term is the product of the downward transition rates $\hat{q}_{i,i-1}$ from $i = N$ to $n+1$ and the second term is the product of the upward transition rates $\hat{q}_{i,i+1}$ from $i = 1$ to $n-1$. The stationary probability distribution $\boldsymbol{\pi} = (\pi_n)$ can thus be written as

$$\pi_n = \frac{z_n}{\sum_{n-1}^{N} z_n}$$

and, furthermore, the stationary probability of the modified Markov chain being in state $N_O = 1$ is

$$\pi_1 = \left\{ 1 + \sum_{n=1}^{N-1} \left[\frac{(N-1)!}{(n+1)!(N-1-n)!} \prod_{i=1}^{n} \hat{c}_i^{\eta} \right] \right\}^{-1} \tag{20}$$

where $\hat{c}_i = \hat{c}_\infty + i\hat{c}_*$ and $\hat{c}_\infty = c_\infty / K$ and $\hat{c}_* = c_* / K$ are the dimensionless background $[Ca^{2+}]$ and dimensionless coupling strength, respectively (Eq. (17)). Finally, the mean first passage time to absorption can be calculated as the inverse of the steady-state probability flux, which in its dimensional form is $k_{\text{attrit}} = q_{10}\pi_1$ where $q_{10} = k^-$ (Eq. (2)). The stochastic attrition time constant is thus $\tau_{\text{attrit}} = 1/k_{\text{attrit}} = 1/\text{k}_-\pi_1$ as shown in Eq. (19).

While Hill's diagrammatic method is also applicable when the initial number of open channels is $N_O = N$, the analytical formula (not shown) becomes more cumbersome due to the cycle present in the modified transition-state diagram (Fig. 10C). In this case, we have found it more convenient to numerically calculate the expected time to stochastic attrition using Eq. (14).

References

[1] N. Allbritton, T. Meyer, L. Stryer, Range of messenger action of Ca^{2+} ion and inositol 1,4,5-trisphosphate, Science 258 (1992) 1812–1815.
[2] S. Asmussen, M. Bladt, Renewal theory and queueing algorithms for matrix-exponential distributions, in: S. Chakravarthy, A. Alfa (Eds.), Matrix-Analytic Methods in Stochastic Models, Marcel Dekker Inc., New York, 1997, pp. 313–341.
[3] M. Berridge, Inositol trisphosphate and Ca^{2+} signaling, Nature 361 (1993) 315–325.
[4] M. Berridge, Elementary, Global aspects of Ca^{2+} signalling, J. Physiol. 499 (1997) 291–306 (London).
[5] M. Berridge, Neuronal Ca^{2+} signaling, Neuron 21 (1998) 13–26.
[6] D. Bers, Cardiac excitation-contraction coupling, Nature 415 (2002) 198–205.
[7] I. Bezprozvanny, J. Watras, B. Ehrlich, Bell-shaped Ca^{2+}-response curves of Ins(1,4,5)P3- and Ca^{2+}-gated channels from endoplasmic reticulum of cerebellum, Nature 351 (1991) 751–754.
[8] M. Bootman, P. Lipp, Ringing changes to the 'bell-shaped curve', Curr. Biol. 9 (1999) R876–R878.

[9] M. Cannell, H. Cheng, W. Lederer, The control of calcium release in heart muscle, Science 268 (1995) 1045–1049.
[10] H. Cheng, M. Lederer, W. Lederer, M. Cannell, Ca^{2+} sparks and $[Ca^{2+}]_i$ waves in cardiac myocytes, Am. J. Physiol. 270 (1996) C148–C159.
[11] H. Cheng, W. Lederer, M. Cannell, Ca^{2+} sparks: elementary events underlying excitation-contraction coupling in heart muscle, Science 262 (1993) 740–744.
[12] D. Colquhoun, A. Hawkes, A *Q*-matrix cookbook: how to write only one program to calculate the single-channel and macroscopic predictions for any kinetic mechanism, in: B. Sakmann, E. Neher (Eds.), Single-Channel Recording, Plenum Press, New York, 1995, pp. 589–633.
[13] M. Fill, J. Copello, Ryanodine receptor calcium release channels, Physiol. Rev. 82 (2002) 893–922.
[14] C. Franzini-Armstrong, F. Protasi, V. Ramesh, Shape, size, and distribution of Ca^{2+} release units and couplons in skeletal and cardiac muscles, Biophys. J. 77 (1999) 1528–1539.
[15] R. Hagar, A. Burgstahler, M. Nathanson, B. Ehrlich, Type III IP_3 receptor channel stays open in the presence of increased Ca^{2+}, Nature 396 (1998) 81–84.
[16] T. Hill, Free Energy Transduction in Biology and Biochemical Cycle Kinetics, New York, Springer-Verlag, 1989.
[17] R. Hinch, A mathematical analysis of the generation and termination of calcium sparks, Biophys. J. 86 (2004) 1293–1307.
[18] G. Latouche, V. Ramaswami, Introduction to Matrix Analytic Methods in Stochastic Modeling., Society for Industrial and Applied Mathematics, Philadelphia, PA, 1999.
[19] D. Mak, J. Foskett, Single-channel kinetics, inactivation, and spatial distribution of inositol trisphosphate (IP_3) receptors in Xenopus oocyte nucleus, J. Gen. Physiol. 109 (1997) 571–587.
[20] J. Marchant, I. Parker, Kinetics of elementary Ca^{2+} puffs evoked in Xenopus oocytes by different Ins(1,4,5)P3 receptor agonists, Biochem. J. 334 (1998) 505–509.
[21] B. Mazzag, C. Tignanelli, G. Smith, The effect of residual Ca^{2+} on the stochastic gating of Ca^{2+}-regulated Ca^{2+} channels, J. Theor. Biol. 235 (2005) 121–150.
[22] I. Moraru, E. Kaftan, B. Ehrlich, J. Watras, Regulation of type 1 inositol 1,4, 5-trisphosphate-gated Ca^{2+} channels by IP_3 and Ca^{2+}: simulation of single channel kinetics based on ligand binding and electrophysiological analysis, J. Gen. Physiol. 113 (1999) 837–849.
[23] V. Nguyen, The Dynamics of Ca^{2+} Puffs: A Study of Instantaneously Coupled Intracellular Ca^{2+} Channels, The College of William and Mary, Williamsburg, VA, 2005.
[24] V. Nguyen, R. Mathias, G. Smith, A stochastic automata network descriptor for markov chain models of instantaneously-coupled intracellular Ca^{2+} channels, Bull. Math. Biol. 67 (2005) 393–432.
[25] E. Niggli, Localized intracellular Ca^{2+} signaling in muscle: Ca^{2+} sparks and Ca^{2+} quarks, Annu. Rev. Physiol. 61 (1999) 311–335.
[26] J. Norris, Markov Chains, Cambridge University Press, Cambridge, 1997.
[27] I. Parker, J. Choi, Y. Yao, Elementary events of IP_3-induced Ca^{2+} liberation in Xenopus oocytes: hot spots, puffs and blips, Cell Calcium 20 (1996) 105–121.
[28] J. Ramos-Franco, M. Fill, G. Mignery, Isoform-specific function of single inositol 1,4,5-trisphosphate receptor channels, Biophys. J. 75 (1998) 834–839.
[29] J. Rengifo, R. Rosales, A. Gonzalez, H. Cheng, M. Stern, E. Rios, Intracellular Ca^{2+} release as irreversible Markov process, Biophys. J. 83 (2002) 2511–2521.
[30] E. Rios, M. Stern, Ca^{2+} in close quarters: microdomain feedback in excitation-contraction coupling and other cell biological phenomena, Annu. Rev. Biophys. Biomol. Struct. 26 (1997) 47–82.
[31] J. Sham, L. Song, Y. Chen, L. Deng, M. Stern, E. Lakatta, H. Cheng, Termination of Ca^{2+} release by a local inactivation of ryanodine receptors in cardiac myocytes, Proc. Natl. Acad. Sci. U.S.A. 95 (1998) 15096–15101.
[32] J. Shuai, P. Jung, Stochastic properties of Ca^{2+} release of inositol 1,4,5-trisphosphate receptor clusters, Biophys. J. 83 (2002) 87–97.
[33] J. Shuai, P. Jung, Optimal ion channel clustering for intracellular calcium signalling, Proc. Natl. Acad. Sci. U.S.A. 100 (2003) 506–510.
[34] G. Smith, Modeling the stochastic gating of ion channels, in: C. Fall, E. Marland, J. Wagner, J. Tyson (Eds.), Computational Cell Biology, Springer-Verlag, 2002, pp. 291–325.
[35] G. Smith, L. Dai, R. Muira, A. Sherman, Asymptotic analysis of equations for the buffered diffusion of intracellular Ca^{2+}, SIAM J. Appl. Math. 61 (2001) 1816–1838.
[36] M. Stern, Theory of excitation-contraction coupling in cardiac muscle, Biophys. J. 63 (1992) 497–517.
[37] M. Stern, H. Cheng, Putting out the fire: what terminates calcium-induced calcium release in cardiac muscle? Cell Calcium 35 (2004) 591–601.
[38] M. Stern, L. Song, H. Cheng, J. Sham, H. Yang, K. Boheler, E. Rios, Local control models of cardiac excitation-contraction coupling. A possible role for allosteric interactions between ryanodine receptors, J. Gen. Physiol. 113 (1999) 469–489.
[39] W. Stewart, Introduction to the Numerical Solution of Markov Chains, Princeton University Press, Princeton, 1994.
[40] X. Sun, N. Callamaras, J. Marchant, I. Parker, A continuum of IP_3-mediated elementary Ca^{2+} signalling events in Xenopus oocytes, J. Physiol. 509 (1998) 67–80.
[41] S. Swillens, P. Champeil, L. Combettes, G. Dupont, Stochastic simulation of a single inositol 1,4,5-trisphosphate-sensitive Ca^{2+} channel reveals repetitive openings during 'blip-like' Ca^{2+} transients, Cell Calcium 23 (1998) 291–302.
[42] S. Swillens, G. Dupont, L. Combettes, P. Champeil, From Ca^{2+} blips to Ca^{2+} puffs: theoretical analysis of the requirements for interchannel communication, Proc. Natl. Acad. Sci. U.S.A. 96 (1999) 13750–13755.
[43] C. Tignanelli, The Effect of Residual Ca^{2+} on the Stochastic Gating of Ca^{2+}-Regulated Ca^{2+} Channels, The College of William and Mary, Williamsburg, VA, 2005.
[44] S. Wang, M. Stern, E. Rios, H. Cheng, The quantal nature of Ca^{2+} sparks and in situ operation of the ryanodine receptor array in cardiac cells, Proc. Natl. Acad. Sci. U.S.A. 101 (2004) 3979–3984.
[45] Y. Yao, J. Choi, I. Parker, Quantal puffs of intracellular Ca^{2+} evoked by inositol trisphosphate in Xenopus oocytes, J. Physiol. 482 (1995) 533–553.